Characteristics of a charged-coupled-device-based optical mapping system for the study of cardiac arrhythmias

David Tang
Yuhua Li
Jessica Wong
University of Oklahoma
Center for Bioengineering and School of Electrical Engineering and Computer Engineering
Norman, Oklahoma 73019

Sunny Po
Eugene Patterson
University of Oklahoma Health Science Center
Cardiac Arrhythmia Research Institute
Oklahoma City, Oklahoma 73104

Wei R. Chen
University of Central Oklahoma
Department of Physics and Engineering
100 N. University Drive, Edmond, Oklahoma 73034

Warren Jackman
University of Oklahoma Health Science Center
Cardiac Arrhythmia Research Institute
Oklahoma City, Oklahoma 73104

Hong Liu
University of Oklahoma
Center for Bioengineering and School of Electrical Engineering and Computer Engineering
Norman, Oklahoma 73019
E-mail: Liu@ou.edu

Abstract. We develop an optical fluorescent mapping system that is able to record the action potential wavefront propagation within cardiac tissue samples with high spatial and temporal resolutions. The system's main component, the fluorescence acquisition device (customized CCD camera), offers a high spatial resolution of 128×128 pixels, with 12-bit digitization and a frame rate of 490 frames/s. The system is designed and implemented to image an area of approximately 20×20 mm at its minimum object distance of 140 mm, corresponding to a spatial resolution of approximately 3 line pairs/mm. Experiments using this system with di-4-ANEPPS-stained canine cardiac tissues with stimulated action potentials through external electrodes result in successful mappings of the distribution and propagation of the action potential wavefronts, showing the system's sensitivity to the change in fluorescence intensity in regions of action potentials. These data demonstrate this optical mapping system as a powerful device in the study of cardiac arrhythmia mechanisms.
 [DOI: 10.1117/1.1896007]

Keywords: optical mapping; charge-coupled devices; spatial resolution; temporal resolution; dynamic range; optical filters.

Paper 03081 received Jun. 19, 2003; revised manuscript received Oct. 6, 2004; accepted for publication Oct. 13, 2004; published online Apr. 11, 2005.

1 Introduction

Cardiac arrhythmias are the results of irregularities in the action potential wavefront propagations within the heart tissue. For instance, during myocardial infarctions, a leading cause of ventricular tachyarrhythmia, a significant amount of scars are deposited across the cardiac tissue. These scars distort the normal orientations and connections of the myocardial fibers. Although the surviving myocytes are able to generate normal action potentials, slow conduction velocity and distorted propagation paths have been observed.[1–3] Due to the complexity of the wavefront distributions and high propagation velocities of the action potential, in the study of the cardiac arrhythmia phenomenon a high spatial and temporal resolution technique is required to accurately map the action potential wavefront propagation and distribution within cardiac tissues.[4,5]

Optical mapping using voltage-sensitive dyes has become a prominent technique in the study of electrical activities within cardiac tissues. The technique can be carried out with devices that can acquire optical signals with both high spatial frequency and high temporal frequency. Currently, two devices dominate the field, charge-coupled devices (CCDs) and photo diode arrays (PDAs). Both optical mapping techniques possess advantages and disadvantages. However, due to the unique ability of CCD detectors in offering both high spatial resolution and temporal resolution, it has been selected as the detector of choice. The objective of this investigation is to design and to implement an optical mapping system using a CCD detector as its main component, and to validate the system through characterization and experiments in optical mapping of action potentials in cardiac tissue.

2 Background

2.1 *Optical Mapping*

A number of techniques have been applied to investigate the propagation of action potential within cardiac tissues. Techniques such as using patch clamps provide meticulous information regarding the ionic currents across the membranes, but do not offer information regarding the interaction between cells. Multielectrode recordings provide reasonable spatial resolution but not the time course of action potential propa-

Address all correspondence to Professor Hong Liu, University of Oklahoma, 202 West Boyd Street, Room 219, Norman OK 73019.

1083-3668/2005/$22.00 © 2005 SPIE

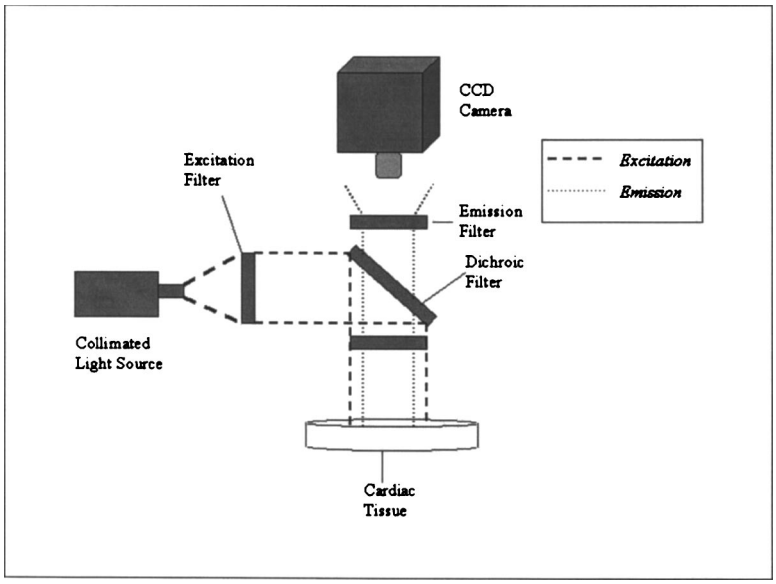

Fig. 1 Optical mapping system. Light from the halogen light source is filtered by the excitation filter and reflected by the dichroic mirror onto the tissue sample. The induced fluorescence from the di-4-anepps molecules, bonded to the tissue sample, is then filtered twice through the dichroic filter and then through the emission filter before reaching the CCD detector.

gations. Optical mapping techniques, although relatively new, have the ability to provide both high spatial resolution and temporal resolution.[6–9]

Optical mapping systems are generally composed of specialized illumination and detection instruments with a variety of characteristics depending on the application. In this paper, stained cardiac tissue preparations are illuminated with a chosen light source. The light source is filtered to select the optimal excitation wavelengths for the specific dye chosen to convert transmembrane potentials into optical signals. Fluorescent light from the preparation, due to the excitation by the illumination, is filtered to remove the background-reflected light before reaching the CCD detector. The CCD detector is placed in the objective image plane and acquires the final optical signals. The signal is then processed and stored by a frame grabber.[10–19]

3 Methodology

3.1 *Optical Mapping System*

A digital imaging system setup was designed to map the action potential propagation within a piece of cardiac tissue with dimensions of 20×20 mm. A detailed representation of the setup is shown in Fig. 1. The system consists of a 150-W quartz halogen light source, a fiber optic light guide, an emission filter, an excitation filter, a dichroic filter, and a custom CCD imager.

3.2 *CCD Imager*

The spatial complexity of the propagating wavefront dictates the spatial resolution requirements for the CCD detector. However, it is often difficult to know, before hand, the spatial complexity of wavefronts, thus making it difficult to decide on a minimum spatial resolution. Independent of wavefront complexity, with a spatial resolution of 1 mm or lower, many cells will contribute to the light signals acquired by an individual detector element and to the optical action potential. This can result in blurring of the action potential. Therefore, a photodetector with a spatial resolution significantly higher than 1 mm is required. However, without adequate temporal resolution, it is impossible for any detector, no matter how high the spatial resolution, to accurately acquire an action potential wavefront propagation.

The temporal resolution requirement of the detector is dictated mainly by the propagation velocity of the action potential within the tissue preparation. The wavefront propagation in cardiac tissues has an average velocity around 0.5 m/s, with individual velocities ranging from 0.1 to 1 m/s. With a 20 ×20-mm tissue preparation, an action potential starting at one corner of the tissue with a velocity of 0.5 m/s will take approximately 28 ms to traverse to the opposite corner. It will take a photodetector with a minimum frame rate of 36 frames/s (1/28 ms) to capture the propagation. The detailed information of action potential propagation requires higher temporal resolution.

Another factor involved in setting a standard for temporal resolution is the temporal characteristic of the individual action potential. Experiments using floating microelectrode recordings from the epicardial surface of guinea pig ventricle showed[20] that approximately 90% of action potential signal was below 150 Hz. Since sampling theory requires a rate of at least twice the highest frequency component of a given signal for its correct reconstruction, a CCD detector with a sampling rate at least greater than 300 frames/s is necessary.

The dynamic range of the photodetector is also a crucial factor. A low dynamic range makes it difficult to capture large background fluorescence while providing adequate voltage resolution for the action potential. This is important because the total fluorescence measured consists mostly, around 90%, of background fluorescence. A system with high temporal and spatial resolutions but low dynamic range will not be able to distinguish between noise and changes in signal intensity due

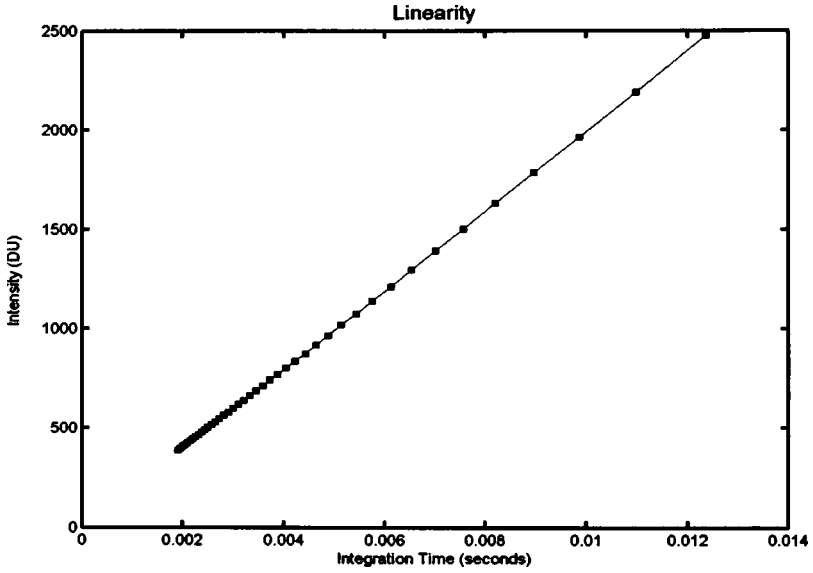

Fig. 2 Linearity curve. The output intensity in digital units is linearly proportional to the integration time.

to the propagation of the action potential wave front.

Taking account of the preceding considerations, a CCD chip with 128×128 pixels, each pixel having a dimension of 0.016×0.016 mm (Dalsa, Ontario, Canada), was selected. With dedicated readout electronics, the CCD detector system provides a frame rate of 490 frames/s and 12-bit digitization. The lens system was designed to image an area of approximately 20×20 mm at its minimum object distance. A 25-mm/f-0.95 lens was chosen. It utilizes a C-mount connection. The resulting lens setup has a demagnification ratio of 9.2:1, and a spatial resolution of 3.2 line pairs/mm with an image area of 20×20 mm at its minimum object-image conjugate.

3.3 *Optical Filters*

The fast fluorescence dye di-4-ANEPPS as the mapping agent was selected for the experiment. Di-4-ANEPPS is a voltage-sensitive, fast dye used in detecting the action potential across all, or portions of, the membranes of nerve and cardiac muscle cells. It has a high SNR and a relatively high fluorescent change in the presence of a change in voltage[21–26] (~10% per 100 mV). Di-4-ANEPPS has an absorption maximum around 475 nm and an emission maximum around 617 nm. Designed in accordance with the dye absorption/emission characteristics, the excitation filter is a bandpass filter (480±30 nm), the emission filter is a bandpass filter (635±27.5 nm), and the dichroic filter transmits light only with a wavelength above 550 nm.

3.4 *System Characterization*

The performance of the system must be evaluated. Because CCD detectors have different responses to different wavelengths of light, all the illuminations used in the evaluation experiments were filtered to approximate the wavelengths given off by Di-4-ANEPPS dye molecules during fluorescence.

3.4.1 *Linearity*

Linearity is one of the most important characteristics of the optical mapping system. To be able to accurately acquire fluorescence signals and to study their behaviors, the optical mapping system must have as close to a linear relationship as possible between the input intensity of the light photons and its digital output. To test the linearity of the optical system, a series of frames of a uniformly illuminated constant field were taken, with variations in integration time for each individual frame. Because the camera under inspection does not have the ability to allow the control of the integration time, different frame rates were used to acquire the frames. The readout time was then subtracted from the acquisition time of each frame to deduce the integration time for each particular frame:

$$\frac{1}{\text{frame rate}}(1 \text{ frame}) - \text{frame transfer time}(133.9\ \mu\text{s}) = \text{integration time}. \quad (1)$$

A series of frames were acquired at a frame rate ranging from 30 to 490 frames/s in 10-frame/s intervals. Along with the images, dark images were also acquired at each individual frame rate. The dark image was then subtracted from the corresponding image to remove the offset dark current. The mean was then calculated over a 10×10-pixel region in the center of the processed image. The final result is plotted as a function of integration time in Fig. 2.

3.4.2 *Spatial resolution and contrast transfer function*

To determine the spatial resolution of the entire optical mapping system, a target U.S. Air Force (USAF) 2×2-in. NEG made by Edmund Industrial Optics was imaged and the contrast transfer function (CTF) was calculated using the following equation:

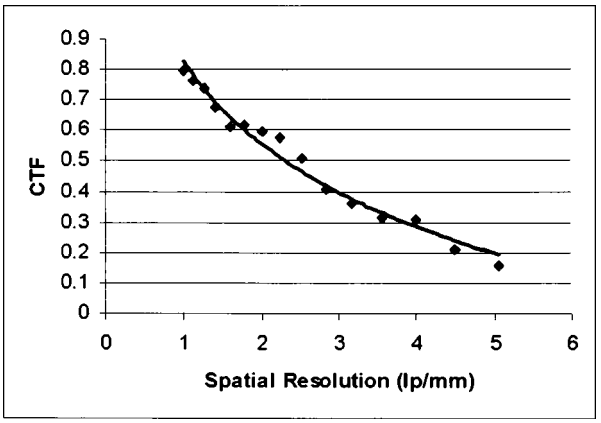

Fig. 3 CTF versus the spatial resolution of the system.

$$\mathrm{CTF}=\frac{I_{\max}-I_{\min}}{I_{\max}+I_{\min}}, \tag{2}$$

where $I_{\max}$ and $I_{\min}$ are maximum and minimum signals, respectively. The resulting curve is shown in Fig. 3.

3.4.3 *Photon transfer curve*

The photon transfer technique has proven to be one of the most valuable CCD transfer curves for calibrating, characterizing, and optimizing system performance. Every component in a CCD camera must work correctly in order to produce a photon transfer curve with the right characteristics. The photon transfer curve is a plot of signal $S(\mathrm{DN})$ versus noise $\sigma_S(\mathrm{DN})$ for the optical mapping system, where DN is dark noise.

In our experiment, 50 frames were acquired at a frame rate ranging from 30 to 490 frames/s in 10-frame/s intervals. To improve the statistics for the photon transfer data, the 50 frames taken at the same illumination level were averaged. Then, $S(\mathrm{DN})$ was determined by calculating the mean of the resulting image.

Noise data for the ordinate were determined by calculating the standard deviation of the region of pixels after pixel-to-pixel nonuniformity was removed. Pixel nonuniformity was eliminated by simply differencing two identical images taken back to back at the same exposure level. The variance, $\sigma_S^2(\mathrm{DN})$, of this differenced frame was given by

$$\sigma_S^2(\mathrm{DN})=\frac{\sum_{i=1}^{N_{\mathrm{pix}}}[S_i(\mathrm{DN})-S(\mathrm{DN})]^2}{2N_{\mathrm{pix}}}, \tag{3}$$

where $S_i(\mathrm{DN})$ is the signal of i'th pixel of the first image, $S(\mathrm{DN})$ is the mean signal of the two images, and N_{pix} is the number of pixels of one image.

A factor of 2 must be included in the denominator because when two identical frames are either subtracted or added, the random noise component (the standard deviation) of the resultant frame increases by a square root of 2. To improve the statistics for the noise data, the actual noise $\sigma_S(\mathrm{DN})$ was determined by first differencing frames 1 and 2, then frames 2 and 3, and so on with the last differencing being between the first frame and the very last frame. These values were then averaged to yield the final noise $\sigma_S(\mathrm{DN})$. The final curve is shown in Fig. 4. The averaged curve, the solid line, is enveloped between two additional dashed curves, which are the maximum and minimum limits derived from all the series of photon transfer curves calculated without averaging.

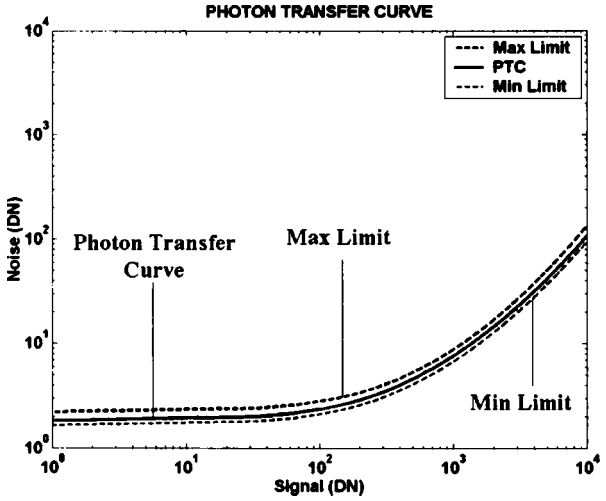

Fig. 4 Photon transfer curve. The curve is initially flat, where DN dominates. The curve then takes on a slope of 1/2 due to shot noise. The final section of the curve has a slope of 1 governed by noises caused by pixel nonuniformities.

The behavior of the optical mapping system's photon transfer curve is normal, which is an excellent indication that the system works properly. In Fig. 4, the curve is flat when the signal is low (in analog digital units [ADU]). This area is independent of the signal intensity, thus the slope is close to 0. Furthermore, the read noise in this area is very small, less than 10 ADU. In the main body of the curve where shot noise dominates, the slope of the line is close to 1/2. Shot noise represents the noise associated with the random arrival of photons on the CCD, it is proportional to the square root of the number of incident photons, hence the slope of 1/2. The third and final region of the curve is governed by the fixed pattern noise that is the result of variations in sensitivity among detector elements. Noise from pixel nonuniformity is proportional to the signal intensity, and is represented by the slope of 1.

3.5 *Experiments with Tissue Samples*

A canine cardiac tissue sample approximately 25×25 mm was harvested from an adult mongrel dog. The tissue was placed within a constant-flow perfusion apparatus immersed with 37 °C Tyrode's solution (mmol/L: NaCl 123, KCl 5.4, $NaHCO_3$ 22, NaH_2PO_4 0.65, $MgCl_2$ 0.5, glucose 5.5, $CaCl_2$ 2.0 bubbled with 95% O_2 and 5% CO_2 gas mixture). To reduce motion artifacts in the optical recordings, cytochalasin D at concentration of approximately 25 μmol/L was added to the solution, since light scattering caused by mechanical contraction could distort the optical signals of the action potentials. Cytochalasin D has been shown to effectively suppress the cardiac contractile force without significantly altering the action potential characteristics.[27]

After perfusion with the 37 °C Tyrode's solution, 5 mg of di-4-ANEPPS dissolved in 4 ml of dimethyl sulfoxide (DMSO) was added to the perfusate to achieve a final con-

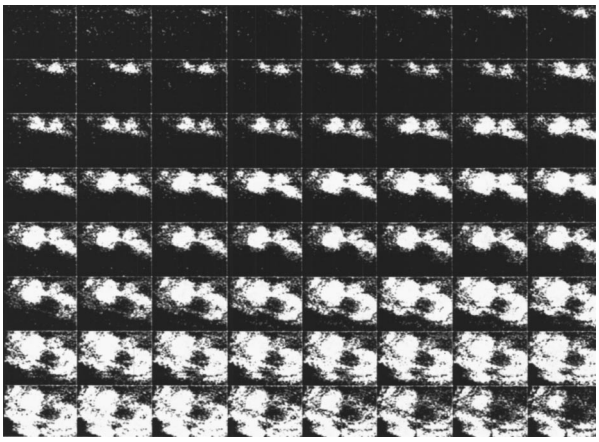

Fig. 5 Optical mappings of action potential propagations within a canine cardiac tissue sample. Each frame consists of 128×128 pixels, imaging an area of approximately 20×20 mm. The signals were collected with a temporal resolution around 2 ms. The stimulation was applied at the top right corner of the tissue sample. The cycle consists of 64 consecutive frames acquired over a period of approximately 131 ms.

centration of 2 μmol/L. Following the staining with Di-4-ANEPPS, the tissue preparation was again perfused with 37 °C Tyrode's solution containing 20 μmol/L of cytochalasin D. The final size of the preparation was approximately 20×20 mm. Continued perfusion with warm Tyrode's solution was used throughout the experiment.

Light coming from a 150-W quartz halogen light source was first filtered through the excitation filter. The remaining light with a wavelength around the absorbance peak of the di-4-ANEPPS dye (~475 nm) was reflected by the dichroic mirror upon the cardiac tissue preparation. The di-4-ANEPPS dye molecules bonded to the tissue preparation fluoresces under the excitation. The light resulting from the fluorescence (~617 nm) was double-filtered by the emission filter and the dichroic filter, minimizing the noise from extraneous wavelengths (see Fig. 1). The CCD camera received the optical signal and converted it to digital signal, and then the signal was sent to the computer by the frame grabber. During this process, the tissue preparation was paced by a 2× diastolic threshold current, 1 Hz frequency, using a sheathed plunge bipolar electrode and a programmable stimulator.

4 Results

A total of 4900 frames were collected over a period of 10 s. The images showed a periodic pattern, with an approximately 1-Hz frequency. Figure 5 illustrates one of the cycles collected. The illustration consists of 64 individual frames taken consecutively at a frame rate of 490 frames/s, spanning a time period of 131 ms. The images clearly indicate a change in fluorescence level of the di-4-ANEPPS dye molecules under the influence of voltage changes across the cardiac membrane due to the application of electrical stimulations and the resulting action potential propagation. In each frame (around 2-ms temporal resolution), the pattern is determined in a 20 ×20-mm section of left ventricular canine epicardium. The timing sequence starts in the upper left-hand corner and proceeds from left to right, from the uppermost row sequentially to the lowermost row (lower right-hand corner). Depolarization (local activation) is indicated by decreased fluorescence (as depicted by increased brightness in the present recordings). Epicardial activation originated from the bipolar stimulation site (a 4-ms-duration square-wave pulse at 1 Hz) in the upper right-hand corner of the tissue sample. The activation wavefront proceeded slowly in both a clockwise and a counterclockwise direction around a central zone of poorly excitable myocardium (the dark center of each individual frame). The two wavefronts met and extinguished (not shown) in the lower middle portion of the frame. Activation of the tissue took place over approximately 100 ms. Since the tissue dimensions were approximately 20×20 mm, to travel from one corner of the tissue to the other, the action potential wavefront must traverse a distance of approximately 28 mm. With this knowledge, one can calculate the action potential propagation velocity to be ~0.21 m/s, which is within the normal propagation velocity of most cardiac tissues.

To further validate the capabilities of this optical mapping system, the optical signal intensity collected by a single detector element over time was evaluated with respect to microelectrode signals. Figure 6 shows the signal intensity of a chosen pixel (detector element) with respect to time, while Fig. 7 shows the microelectrode recordings of the same events. In the microelectrode recordings, consecutive action potentials are separated by approximately 1300 ms between each initial upstroke (Fig. 6). This pattern is almost identical to the optical signals captured and displayed by the optical mapping system, which also shows a separation close to 1300 ms between initial upstrokes of consecutive action potentials (Fig. 7). These evaluations demonstrated the capabilities of the optical mapping system in mapping the action potential wavefront propagations within cardiac tissue samples with high spatial/temporal resolution and high sensitivity.

5 Conclusion

The study of cardiac arrhythmia mechanisms requires an optical mapping system that can provide high spatial and temporal resolutions and high sensitivity to capture the complex action potential wave propagation within the tissue preparation. An action potential can have a propagation velocity ranging from 0.1 to 1 m/s. For a tissue sample of 20×20 mm, it will take an action potential approximately 28 ms to traverse from one corner to the opposite corner, enough time for an optical detector with a frame rate of 36 frames/s (1/28 ms) to capture the propagation. However, a much higher temporal resolution is required for an optical mapping system to be able to acquire enough data during this 28 ms to enable an accurate study of the wavefront propagation and distribution mechanism.

We designed, constructed, and evaluated a CCD-detector-based optical mapping system for mapping the action potential wavefront propagation across cardiac tissue preparations. The system has competitive characteristics in all three categories: temporal resolution, spatial resolution, and dynamic range. This is important because the detailed information acquired by mapping the action potential wavefront propagations is not dependent solely on either spatial resolution or temporal resolution but on the combination of the two. Dynamic range is also crucial, without an adequate dynamic

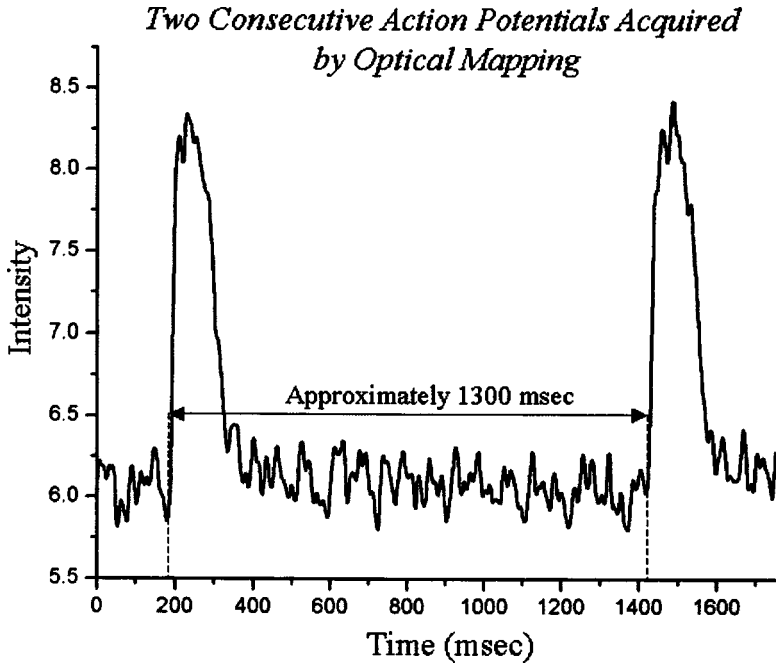

Fig. 6 Consecutive action potentials collected by a single detector element of the optical mapping system.

range, the optical mapping system will not be able to distinguish the small variations in the incoming light intensities due to action potential stimulations. The optical mapping system offers a spatial resolution of 3.22 line pairs/mm, with a temporal resolution of 2.04 ms or 490 frames/s, 128×128 detector elements or pixels with 12-bit digitization, and a dynamic range close to 3000. The customized lens system provides a minimum working distance of 140 mm and optimizes the light collection efficiency with an f-# of 0.95. Although a lens can be custom designed to have an even larger aperture to increase light collection efficiency, it may come at a significantly increased cost.

When tested in action potential wavefront propagation mapping experiments within a tissue preparation of approximately 20×20 mm, the optical mapping system demonstrated its ability to acquire detailed information regarding the propagation of the action potential wavefront and its distribution. It was able to capture 64 frames within 130 ms, the time it took for one action potential wavefront to travel from one corner of the tissue preparation to the opposite corner. Evaluation with microelectrode recordings verified the accuracy of the acquired data.

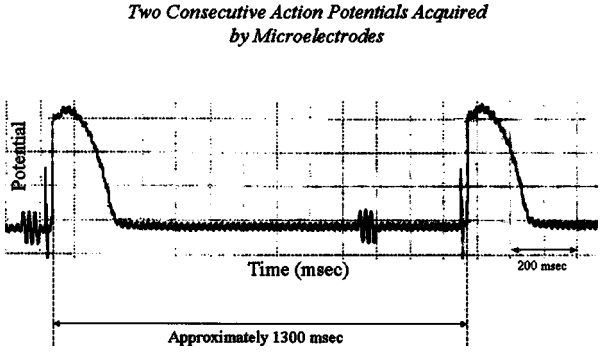

Fig. 7 Simultaneous recordings of events illustrated in Fig. 6 by microelectrodes.

We are currently investigating the possibility of using a dual-CCD setup and the ratiometry techniques. Each CCD camera would selectively acquire light of a specific region of the Di-4-ANEPPS spectrum, taking advantage of the spectrum shift that results from the change in transmembrane potential. The CCD cameras would acquire data simultaneously during an experiment. Data from both cameras would be processed to magnify the variations in signal intensity due to the action potential wavefront propagation.

Acknowledgments

This work was supported in part by grants from the National Institute of Health (RO1 EB-002604, RO1 CA104773) and by a grant from the Dr. Jackson College of Graduate Studies and Research of the University of Central Oklahoma, and by a grant from the National Institute of Health (P20 RR016478 from the INBRE Program of the National Center for Research Resources). The authors would like to acknowledge the support of the Charles and Jean Smith Chair endowment fund as well.

References

1. E. Braunwald, *Heart Disease: A Textbook of Cardiovascular Medicine*, 5th ed., pp. 548–592, W.B. Saunders Company, Philadelphia (1997).
2. J. M. T. De Bakker, F. J. L. Van Capelle, and M. J. Janse, ''Reentry as a cause of ventricular tachyacardia in patients with chronic ischemic heart disease: electrophysiology and anatomic correlation,'' *Circulation* **77**, 589–606 (1998).
3. S. M. Pogwizd and P. B. Corr, ''Electrophysiologic mechanisms underlying arrhythmias due to reperfusion of ischemic myocardium,'' *Circulation* **76**, 404–426 (1987).
4. R. E. Ideker, P. D. Wolf, E. Simpson, E. E. Johnson, S. M. Blanchard et al., ''The ideal cardiac mapping system,'' in *Cardiac Mapping*, M.

Shenasa, M. Borgreffe, G. Breithardt, W. HarverKamp, and G. Hindricks, Eds., pp. 649–653, Futura, Mount Kisco, NY (1993).
5. M. J. Janse, F. J. L. van Cappelle, H. Morsink, A. G. Kleber, F. Wilms-Schopman et al., ''Flow of injury current and patterns of excitation during early ventricular arrhythmias in acute regional myocardial ischemia in isolated porcine and canine hearts,'' *Circ. Res.* **47**, 151–165 (1980).
6. H. Windisch, H. Ahammer, P. Schaffer, W. Muller, and D. Platzer, ''Optical multisite monitoring of cell excitation phenomena in isolated cardiomyocytes,'' *Pfluegers Arch. Gesamte Physiol. Menschen Tiere* **430**(4), 508–518 (1995).
7. L. B. Cohen and S. Lesher, ''Optical monitoring of membrane potential. Methods of multisite optical measurement,'' in *Optical Methods in Cell Physiology*, P. De Weer and B. M. Slazberg, Eds., pp. 71–100, Wiley-Interscience (1986).
8. M. R. Franz, ''Method and theory of monophasic action potential recording,'' *Prog. Cardiovasc. Dis.* **33**, 347–368 (1991).
9. K. R. Laurita, S. D. Girouard, and D. S. Rosenbaum, ''Modulation of ventricular repolarization by a premature stimulus: role of epicardial dispersion of repolarization kinetics demonstrated by optical mapping of the intact guinea pig heart,'' *Circ. Res.* **97**, 493–503 (1996).
10. G. G. Blasdel and G. Salama, ''Voltage-sensitive dyes reveal a modula organization in monkey striate cortex,'' *Nature (London)* **321**, 579–585 (1986).
11. W. T. Baxter, J. M. Davidenko, L. M. Loew, J. P. Wuskell, and J. Jalife, ''Technical features of a CCD video camera system to record cardiac fluorescence data,'' *Adv. Biomed. Eng.* **25**, 713–725 (1997).
12. A. Mishima et al., ''A high-speed optical mapping system to record cardiac action potential,'' in *Engineering in Medicine and Biology Society, 2000, Proc. 22nd Ann. Int. Conf. of the IEEE*, Vol. 2, p. 1286 (2000).
13. S. N. Lu, E. Entcheva, V. Sharma, and L. Tung, ''Optical mapping of anatomical reentry in monolayers of cultured neonatal rat cardiac myocytes,'' in *Proc. 1st Joint BMES/EMBS Conf.*, Vol. 1, p. 139 (1999).
14. S. M. Dillon, T. E. Kerner, J. Hoffman, V. Menz, K. S. Li, and J. J. Michele, ''A system for in-vivo cardiac optical mapping,'' *IEEE Eng. Med. Biol. Mag.* **17**, 95–108 (1998).
15. E.-J. Berbari, P. Lander, D. B. Geselowitz, B. J. Scherlag, and R. Lazzara, ''The methodology of cardiac mapping,'' in *Cardiac Mapping*, M. Shenasa, M. Borggrefe, and G. Breithardt, Eds., pp. 63–77, Futura Publishing, Mount Kisko, NY (1993).
16. P. De Weer and B. M. Salzberg, Eds., *Optical Methods in Cell Physiology*, Wiley, New York (1986).
17. J. R. Janesick, T. Elliott, S. Collins, M. M. Blouke, and J. Freeman, ''Scientific charge-coupled devices,'' *Opt. Eng.* **26**, 692–714 (1987).
18. J. S. Kauer, ''Real time imaging of evoked activity in local circuits of the salamander olfactory bulb,'' *Nature (London)* **331**, 166–168 (1988).
19. N. Lasser-Ross, H. Miyakawa, V. Lev-Ram, S. R. Young, and W. N. Ross, ''High time resolution fluorescence imaging with a CCD camera,'' *J. Neurosci. Methods* **36**, 253–261 (1991).
20. S. D. Girouard, K. R. Laurita, and D. S. Rosenbaum, ''Unique properties of cardiac action potentials recorded with voltage sensitive dyes,'' *J. Cardiovasc. Electrophysiol.* **7**, 1024–1038 (1996).
21. A. Grinvald, R. Hildesheim, I. C. Farber, and L. Anglister, ''Improved fluorescent probes for the measurement of rapid changes in membrane potential,'' *Biophys. J.* **39**, 301–308 (1982).
22. M. Morad and G. Salama, ''Optical probes of membrane potential in heart muscle,'' *J. Physiol. (London)* **292**, 267–295 (1979).
23. G. Salama, ''Optical measurements of transmembrane potential in heart,'' in *Spectroscopic Membrane Probes*, L. M. Loew, Ed., pp. 137–199, CRC Press, Boca Raton, FL (1988).
24. W. Muller, H. Windisch, and H. A. Tritthart, ''Fast optical monitoring of microscopic excitation patterns in cardiac muscle,'' *Biophys. J.* **56**, 623–629 (1989).
25. B. Knisley, ''Transmembrane voltage changes during unipolar stimulation of rabbit ventricle,'' *Circ. Res.* **77**, 1229–1239 (1995).
26. Y. Wu and L. B. Cohen, ''Fast multisite optical measurement of membrane potential,'' in *Fluorescent and Luminescent Probes for Biological Activity: A Practical Guide to Technology for Quantitative Real-Time Analysis*, W. T. Mason, Ed., pp. 389–404, Academic, San Diego, CA (1993).
27. J. Wu, M. Biermann, M. Rubart, and D. P. Zipes, ''Cytochalasin D as excitation-contraction uncoupler for optically mapping action potentials in wedges of ventricular myocardium,'' *J. Cardiovasc. Electrophysiol.* **9**, 1336–1347 (1998).